

Quantum Transport With Two Interacting Conduction Channels

Alexander J. White,¹ Agostino Migliore,^{2, a)} Michael Galperin,¹ and Abraham Nitzan²

¹⁾*Department of Chemistry & Biochemistry, University of California San Diego, La Jolla, CA 92093, USA*

²⁾*School of Chemistry, Tel Aviv University, Tel Aviv, 69978, Israel*

(Dated: 11 January 2021)

The transport properties of a conduction junction model characterized by two mutually coupled channels that strongly differ in their couplings to the leads are investigated. Models of this type describe molecular redox junctions (where a level that is weakly coupled to the leads controls the molecular charge, while a strongly coupled one dominates the molecular conduction), and electron counting devices in which the current in a point contact is sensitive to the charging state of a nearby quantum dot. Here we consider the case where transport in the strongly coupled channel has to be described quantum mechanically (covering the full range between sequential tunneling and co-tunneling), while conduction through the weakly coupled channel is a sequential process that could by itself be described by a simple master equation. We compare the result of a full quantum calculation based on the pseudoparticle non-equilibrium Green function method to that obtained from an approximate mixed quantum-classical calculation, where correlations between the channels are taken into account through either the averaged rates or the averaged energy. We find, for the steady state current, that the approximation based on the averaged rates works well in most of the voltage regime, with marked deviations from the full quantum results only at the threshold for charging the weakly coupled level. These deviations are important for accurate description of the negative differential conduction behavior that often characterizes redox molecular junctions in the neighborhood of this threshold.

PACS numbers: 73.63.-b, 82.20.Xr, 85.65.+h, 82.20.Wt

Keywords: electron tunneling, redox molecular junctions, quantum correlation, rate equations, pseudoparticle nonequilibrium Green functions

I. INTRODUCTION

Transport in mesoscopic and nanoscopic junctions is usually a multichannel phenomenon. Model studies of transport in junctions that comprise two, often interacting, conduction channels have been carried out in order to describe the essential features of different physical phenomena. Prominent examples are studies of interference effects in quantum conduction, analysis of single electron counting, where a highly transmitting junction (a point contact) is used to monitor the electronic state of a poorly transmitting one, and redox molecular junctions, where (transient) electron localization in one channel, stabilized by environmental polarization, determines the transition between redox states that are observed by the conduction properties of another channel. These three classes of phenomena are described by different flavors of the two-channel model. Interference is usually discussed as a single electron problem and interaction with the environment is minimized (often disregarded in model studies) so as to maintain phase coherent transport. Single electron counting with a point-contact detector is by definition a many electron problem, however environmental interactions are again minimized (and again often disregarded in theoretical analysis) by lowering the experimental temperature in order to obtain detectable sig-

nals. Conduction in redox junctions is usually observed in room temperature polar environments and is characterized by large solvent reorganization that accompanies the electron localization at the redox site.

In recent work^{1-3,7} we have studied the conduction properties of junctions of the latter type. We first analyzed, for a model involving a single conduction channel, the consequence of large solvent reorganization in the limit where the coupling between the molecular bridge and the metal leads is large relative to the frequency of the phonon mode used to model the solvent dynamical response.¹⁻³ It was shown (using a mean field description essentially equivalent to the Born Oppenheimer approximation) that solvent induced stabilization of different charging states of the molecule can result in multistable operation of the junction, offering a possible rationalization of observations of negative differential resistance (NDR) and hysteretic response in molecular redox junctions. Such multistability was indeed observed recently in numerical simulations that avoid the mean field approximation.^{8,9} Many redox junctions, however, operate in the opposite limit of relatively small molecule-lead coupling, where a single conduction channel model cannot show multistable transport behavior. Two of us have recently advanced a two channel model that can account for such observations.⁷ In the absence of electron-phonon interaction (solvent polarization) this model is given by

^{a)}Present address: Department of Chemistry, Duke University, Durham, NC 27708, USA

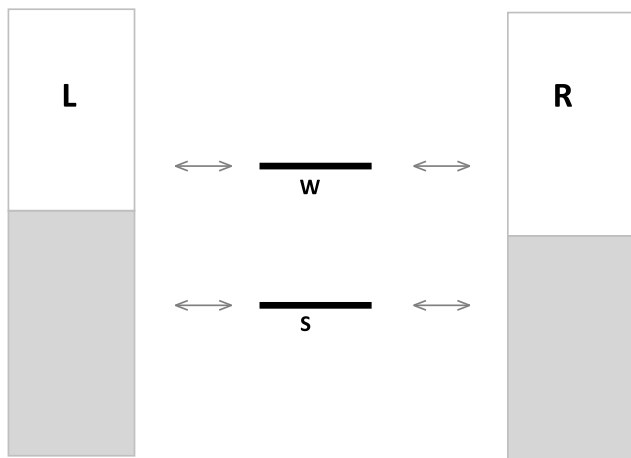


FIG. 1. The two channel model discussed in the paper. Each channel comprises one level coupled to the left and right electrodes. W and S denote weakly and strongly coupled levels, respectively.

the Hamiltonian (see Fig. 1)

$$\begin{aligned} \hat{H} = & \sum_{m=S,W} \varepsilon_m \hat{d}_m^\dagger \hat{d}_m + U \hat{n}_S \hat{n}_W + \sum_{k \in L,R} \varepsilon_k \hat{c}_k^\dagger \hat{c}_k \\ & + \sum_{k \in L,R} \left(V_{kW} \hat{c}_k^\dagger \hat{d}_W + H.c. \right) \\ & + \sum_{k \in L,R} \left(V_{kS} \hat{c}_k^\dagger \hat{d}_S + H.c. \right) \end{aligned} \quad (1)$$

where \hat{d}_m^\dagger (\hat{c}_k^\dagger) creates electron in level m (state k of the contact), and $\hat{n}_m = \hat{d}_m^\dagger \hat{d}_m$, $m = S, W$. In this model, the two channels are coupled only capacitively (no inter-channel electron transfer). U represents the standard Coulomb interaction between them. Two coupled channel models such as (1) also characterize single electron counting devices,^{10–15} where the current in a point contact (that can be represented by channel S) measures the charging state of a quantum dot used as a bridge in a nearby junction (channel W). The noise properties of such junctions have been studied extensively.^{16–21}

In this model, supplemented by electron phonon coupling that represents the response of a polar environment to the electronic occupations in levels W and S , the molecular redox site dominates the properties of one channel (addressed below as “weakly coupled” or “slow” and denoted by W), characterized by strong transient localization stabilized by large reorganization of the polar environment and weak coupling to the metal leads. Transport through this channel, that is, charging and discharging of the molecular redox site, was described by sequential kinetic processes. A second channel (addressed below as “strongly coupled” or “fast” and denoted by S) is more strongly coupled to the leads and is responsible for most or all of the observed current.²² Switching between charging states of the slow channel

amounts to molecular redox states that affect the transmission, therefore the observed current, through the fast channel. Bistability and hysteretic response on experimentally relevant timescales are endowed into the model in a trivial way²³ and, as was shown in Ref. 7 (see also Refs. 24–26), NDR also appears naturally under suitable conditions.

Obviously, this behavior is generic and results from the timescale separation between the W and S channels together with the requirement that the observed current is dominated by the S channel. In Refs. 7 and 27, we have described the expected phenomenology of such junction model in the limit where transport through both channels is described by simple kinetic equations with Marcus electron transfer rates. While, as indicated above, it is natural to model the slow dynamics (observed timescales $\sim 10^{-6}$ s) in this way, it is also of interest to consider fast channel transport on timescales where transport coherence is maintained. For example, one could envision a redox junction that switches between two conduction modes, which shows interference pattern associated with the structure of the fast channel. As a prelude for such considerations, we have studied in Ref. 27 also a model in which the weakly coupled channel W is described by Marcus kinetics, however conduction through the strongly coupled channel S is described as a coherent conduction process by means of the Landauer formula, assuming that the timescale of transport through this channel is fast enough to make it possible to ignore any interaction with the polar environment. As in any mixed quantum-classical dynamics, such description is not consistently derived from a system Hamiltonian, and ad-hoc assumptions about the way the quantum and classical subsystems interact with each other must be invoked, as described in Section II.

In this paper we present a full quantum calculation of the current-voltage response of the two channel model described above, and use it to assess the approximate solution obtained using Eqs. (2)-(6) with models A and B (see Section II). The quantum calculation is done with the pseudoparticle non-equilibrium Green function (PP-NEGF) technique,^{28–31} named the slave boson technique when applied to a 3-states system (Anderson problem at infinite U),^{32–35} which was recently used by two of us to study effects of electron-phonon and exciton-plasmon interactions in molecular junctions.^{36,37} We note that all the methods used in the paper have their own limitations. In particular, PP-NEGF is perturbative in the system-bath coupling. However, it accounts exactly for the intra-system interactions, and it is the role of these interactions (quantum correlations due to system channels interactions) which is missed by the mixed quantum classical approaches and is the focus of the present study.

In Section II we present our model, briefly review the master equation description and introduce two approximate descriptions of mixed classical-quantum dynamics. The PP-NEGF technique and other details of the fully quantum calculation are described in Section III. Sec-

tion IV presents our results and discusses the validity of the approximate calculations. Section V concludes.

II. MIXED QUANTUM CLASSICAL APPROXIMATIONS

To account for the current-voltage behavior of a junction characterized by the Hamiltonian (1), several workers^{16–21} have used a master equation level of description, whereupon, for a given voltage, the dynamics of populating and de-populating the levels S and W is described by classical rate equations involving only their populations, with occupation and de-occupation rates given by standard expressions (see Eq. (4) below). Here, in order to focus on redox junction physics, the coupling of channel W to the contacts is assumed to be much smaller than that of channel S , so that in the absence of correlations channel W can be assumed to be classical and treated within such rate equations approach. At the same time channel S will be treated as quantum, as discussed in the previous section.

In Ref. 27, we have assumed that on the timescale of interest the junction can be in two states: 1 and 0, where the weakly coupled channel, that is the molecular redox site - is occupied or vacant, respectively. The probability $P_1 = 1 - P_0$ that the junction is in state 1 satisfies the kinetic equation

$$\frac{dP_1}{dt} = (1 - P_1) k_{0 \rightarrow 1} - P_1 k_{1 \rightarrow 0} \quad (2)$$

where the rates $k_{0 \rightarrow 1}$ and $k_{1 \rightarrow 0}$ are electron transfer rates between a molecule and an electrode, here the rates to occupy and vacate the redox molecular site, respectively. These rates are sums over contributions from the two electrodes

$$k_{i \rightarrow j} = k_{i \rightarrow j}^{(L)} + k_{i \rightarrow j}^{(R)}; \quad i, j = 0, 1 \quad (3)$$

and depend on the position of the redox molecular orbital energy ε_r relative to the Fermi energy (electronic chemical potential) of the corresponding electrode. In Ref. 27 we have used Marcus heterogeneous electron transfer theory to calculate these rates, thus taking explicitly into account solvent reorganization modeled as electron-phonon coupling in the high temperature and strong coupling limit. For the purpose of the present work it is enough to use the simpler, phonon-less, model

$$\begin{aligned} k_{0 \rightarrow 1}^{(K)}(\varepsilon_r) &= \Gamma_r^K f_K(\varepsilon_r) \\ k_{1 \rightarrow 0}^{(K)}(\varepsilon_r) &= \Gamma_r^K [1 - f_K(\varepsilon_r)] \end{aligned} \quad (4)$$

where ε_r is the energy of the “redox level” (see below), $f_K(E) = [\exp((E - \mu_K)/T) + 1]^{-1}$ ($K = L, R$) is the Fermi-Dirac function of the electrode K , μ_K is the corresponding electronic chemical potential and T is the temperature (in energy units). Γ_r^K , $K = L, R$ are the widths of the redox molecular level due to its electron transfer coupling to the electrodes.³⁸ In terms of the

Hamiltonian, Eq. (1) above, these widths are given by $\Gamma_W^K = 2\pi \sum_{k \in K} |V_{Wk}|^2 \delta(E - \varepsilon_k)$. We have assumed that in the relevant energy regions these widths do not depend on energy.

From Eqs. (2) and (3), the steady state population of the redox site is $P_1 = 1 - P_0 = k_{0 \rightarrow 1} / (k_{0 \rightarrow 1} + k_{1 \rightarrow 0})$, and the current through the weakly coupled channel is $I_W = k_{0 \rightarrow 1}^{(L)} P_0 - k_{1 \rightarrow 0}^{(L)} P_1 = k_{1 \rightarrow 0}^{(R)} P_1 - k_{0 \rightarrow 1}^{(R)} P_0$. This current is however negligible relative to the contribution from the strongly coupled channel. In each of the states 0 and 1, the current I_S as well as the average bridge population $\langle n_S \rangle$ in this channel, are assumed to be given by the standard Landauer theory for a channel comprising one single electron orbital of energy ε_S bridging the leads, disregarding the effect of electron-phonon interaction,^{39,40}

$$I_S(V; \varepsilon_S) = \frac{e}{\hbar} \int_{-\infty}^{+\infty} \frac{d\varepsilon}{2\pi} \frac{\Gamma_S^L \Gamma_S^R [f_L(E) - f_R(E)]}{(\varepsilon - \varepsilon_S)^2 + (\Gamma_S/2)^2} \quad (5)$$

$$\langle n_S(V; \varepsilon_S) \rangle = \int_{-\infty}^{+\infty} \frac{d\varepsilon}{2\pi} \frac{\Gamma_S^L f_L(\varepsilon) + \Gamma_S^R f_R(\varepsilon)}{(\varepsilon - \varepsilon_S)^2 + (\Gamma_S/2)^2} \quad (6)$$

where $\Gamma_S = \Gamma_S^L + \Gamma_S^R$ and where ε_S and Γ_S^K take the values $\varepsilon_S^{(0)}$, $\Gamma_S^{K(0)}$ in state 0, and $\varepsilon_S^{(1)} = \varepsilon_S^{(0)} + U$, $\Gamma_S^{K(1)} = \Gamma_S^{K(0)}$ in state 1. U is essentially a Coulomb energy term that measures the effect of electron occupation in channel W , i.e. at the redox site, on the energy of the bridging orbital in channel S . Γ_S^L , Γ_S^R , ε_S , and U are model parameters. The average population and current in channel S are given by $\langle n_S \rangle = P_0 \langle n_S \rangle^{(0)} + P_1 \langle n_S \rangle^{(1)}$; $\langle I_S \rangle = P_0 I_S^{(0)} + P_1 I_S^{(1)}$, where $I_S^{(0)}$ ($\langle n_S \rangle^{(0)}$) and $I_S^{(1)}$ ($\langle n_S \rangle^{(1)}$) are the values of I_S , Eq. (5) ($\langle n_S \rangle$, Eq. (6)) in system states 0 (redox level empty), and 1 (redox level populated). Finally, the total current at a given voltage is $I = I_S + I_W \approx I_S$.

It should be noted that the rates defined by Eq. (4) are not completely specified, because the “redox energy level” ε_r is not known: it is equal to ε_W only if the capacitive interaction between the S and W channels is disregarded. To take this interaction into account, two models were examined in Ref. 27:

Model A. The rates are written as weighted averages over the populations 0 and 1 of channel S with respective weights $1 - \langle n_S \rangle$ and $\langle n_S \rangle$:

$$\begin{aligned} k_{0 \rightarrow 1} &= \left(1 - \langle n_S \rangle^{(0)}\right) k_{0 \rightarrow 1}^{(S0)} + \langle n_S \rangle^{(0)} k_{1 \rightarrow 0}^{(S0)} \\ k_{1 \rightarrow 0} &= \left(1 - \langle n_S \rangle^{(1)}\right) k_{0 \rightarrow 1}^{(S1)} + \langle n_S \rangle^{(1)} k_{1 \rightarrow 0}^{(S1)} \end{aligned} \quad (7)$$

where $k_{0 \rightarrow 1}^{(S0)}$, $k_{0 \rightarrow 1}^{(S1)}$ are the rates to occupy and vacate, respectively, the redox site when the fast channel is not occupied, while $k_{0 \rightarrow 1}^{(S1)}$, $k_{1 \rightarrow 0}^{(S1)}$ are the corresponding rates when this channel is occupied. The dependence of these rates on the occupation of the fast channel is derived from the dependence of ε_r in Eq. (4) on the occupation of level S : $\varepsilon_r = \varepsilon_W$ when this level is not occupied, and

$\varepsilon_r = \varepsilon_W + U$ when it is. That is,

$$\begin{aligned} k_{0 \rightarrow 1}^{(K,S0)} &= \Gamma_r^K f_K(\varepsilon_W) \\ k_{1 \rightarrow 0}^{(K,S0)} &= \Gamma_r^K [1 - f_K(\varepsilon_W)] \\ k_{0 \rightarrow 1}^{(K,S1)} &= \Gamma_r^K f_K(\varepsilon_W + U) \\ k_{1 \rightarrow 0}^{(K,S1)} &= \Gamma_r^K [1 - f_K(\varepsilon_W + U)] \end{aligned} \quad (8)$$

Here $K = L, R$.

Model B. The rates are given by Eq. (4), with ε_r calculated as the difference between the energies of two molecular states, one with the redox level populated, $E_1 = (\varepsilon_S^{(0)} + U) \langle n_S \rangle^{(1)} + \varepsilon_2^{(0)} = \varepsilon_S^{(1)} \langle n_S \rangle^{(1)} + \varepsilon_2^{(0)}$ and the other with the redox level empty, $E_0 = \varepsilon_S^{(0)} \langle n_S \rangle^{(0)}$:

$$\varepsilon_r = \left(\varepsilon_S^{(1)} \langle n_S \rangle^{(1)} + \varepsilon_2^{(0)} \right) - \varepsilon_S^{(0)} \langle n_S \rangle^{(0)} \quad (9)$$

These two models are associated with different physical pictures that reflect different assumptions about relative characteristic timescales. Model A assumes that the switching rates between states 0 and 1 follow the instantaneous population in channel S , while model B assumes that these switching rates are sensitive only to the average population $\langle n_S \rangle$. Model B results from a standard Hartree approximation that would be valid if the electronic dynamics in channel W is slow relative to that of channel S (see Appendix). From the discussion above it may appear at first glance to be the case, since transmission through channel W is small, implying that the rates $k_{0 \rightarrow 1}$ and $k_{1 \rightarrow 0}$ are small. However, the electronic process that determines the timescale on which these rates change is not determined by the magnitude of these rates but by the response of the electrodes to changes in ε_r following changes in the bridge level population of the strongly coupled channel. This characteristic time (or times), τ_B , which is bounded below by the inverse electrode bandwidth, may depend also on temperature and the energy dependence of the spectral density, and can be shorter than the timescale of order of Γ_S^{-1} on which population in channel S is changing (note that τ_B is vanishingly short in the wide band limit). In this case model A would provide a better approximation. For comparison, we also present below results for model C, in which the effect of the interaction between the two channels on the electron transfer kinetics in channel W is disregarded so that

$$\begin{aligned} k_{0 \rightarrow 1}^K &= \Gamma_W^K f_K(\varepsilon_W) \\ k_{1 \rightarrow 0}^K &= \Gamma_W^K [1 - f_K(\varepsilon_W)] \end{aligned} \quad (10)$$

while the current through channel S continues to be sensitive to the difference between states 0 and 1, as before.

III. THE PSEUDOPARTICLE GREEN FUNCTION METHOD

Models A and B above represent attempts to partly account for the coupling between channels within the clas-

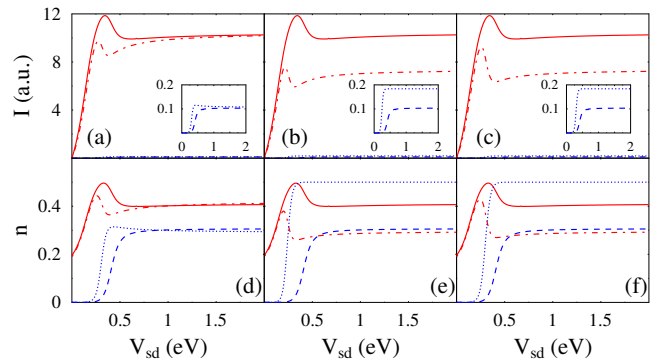


FIG. 2. (Color online) Current (panels a-c) and populations of the channels (panels d-f). Results for the models A (panels a and d), B (panels b and e), and C (panels c and f) are shown for the channels S (dash-dotted line, red) and W (dotted line, blue), and compared to the PP-NEGF results for the same channels (solid, red and dashed, blue lines, respectively). Note, the PP-NEGF data is the same in panels a-c and d-f. See text for parameters.

sical rate equations description of channel W . The existence of capacitive coupling between the channels makes such mixed quantum-classical description potentially invalid, since it misses quantum correlations between the two channels. To estimate the performance of these approximations we shall compare them to a fully quantum calculation based on the pseudoparticle nonequilibrium Green function technique.³⁶

In the PP-NEGF approach, a set of molecular many-body states, $\{|N\rangle\}$, defines the set of pseudoparticles to be considered, so that one pseudoparticle represents each state. In particular, for the model (1) the molecular subspace of the problem is represented by four many-body states: $|N\rangle = |n_W, n_S\rangle$, where $n_{W,S} = 0, 1$. Let \hat{p}_N^\dagger (\hat{p}_N) be the creation (annihilation) operator for the state $|N\rangle$. These operators are assumed to satisfy the usual fermion or boson commutation relations depending on the type of the state. In our case the pseudoparticles associated with the states $|1, 0\rangle$ and $|0, 1\rangle$ are of Fermi type, while those corresponding to states $|0, 0\rangle$ and $|1, 1\rangle$ follow Bose statistics. The PP-NEGF is defined on the Keldysh contour as

$$G_{N_1, N_2}(\tau_1, \tau_2) \equiv -i \langle T_c \hat{p}_{N_1}(\tau_1) \hat{p}_{N_2}^\dagger(\tau_2) \rangle \quad (11)$$

In the extended Hilbert space it satisfies the usual Dyson equation, thereby providing a standard machinery for their evaluation. Reduction to the physically relevant subspace of the total pseudoparticle Hilbert space is achieved by imposing the constraint

$$\sum_N \hat{p}_N^\dagger \hat{p}_N = 1 \quad (12)$$

on the Dyson equation projections. The resulting system of equations for the Green function projections has to be solved self-consistently (see e.g. Ref. 36 for details).

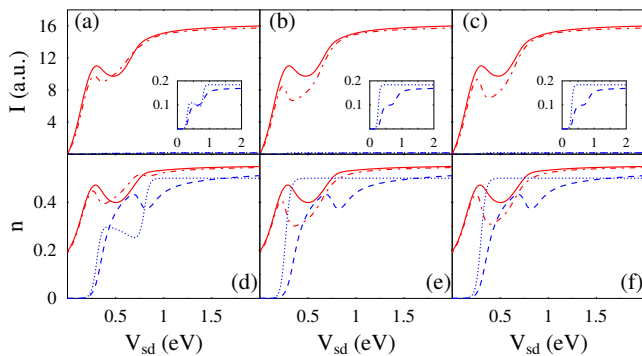


FIG. 3. (Color online) Same as Fig. 2 except $U = 500$ meV

Finally, connections to Green functions of the standard NEGF formulation can be obtained by using relations between the electron operators in the molecular subspace of Eq. (1) and those of the pseudoparticles

$$\hat{d}_m^\dagger = \sum_{N_1, N_2} \langle N_1 | \hat{d}_m^\dagger | N_2 \rangle \hat{p}_{N_1}^\dagger \hat{p}_{N_2} \quad (13)$$

Thus the current through the junction can be obtained either by the usual NEGF expression,⁴⁰ or within its pseudoparticle analog.³⁶

Results of calculations based on this procedure and on the kinetic schemes described in Section I are presented and discussed next.

IV. RESULTS AND DISCUSSION

In Figures 2 and 3 we compare results from the fully quantum calculation based on the PP-NEGF technique with those based on the kinetic approximations defined by models A-C of Section I. Panels (a), (b) and (c) in Fig. 2 show the current through channels S (red) and W (blue) as function of voltage, while the corresponding panels (d), (e) and (f) show, with the same color and line-forms codes, the electronic populations in these channels. The full and dashed lines in these plots correspond to the PP-NEGF calculations for channels S and W , respectively, and are identical in the panels (a-c) and in panels (d-f). The dash-dotted and dotted lines show results based on models A (panels (a) and (d)), B (panels (b) and (e)) and C (panels (c) and (f)). The parameters used in these calculations are $E_F = 0$, $T = 300$ K, $\Gamma_W^L = \Gamma_W^R = 1$ meV, $\Gamma_S^L = \Gamma_S^R = 100$ meV, $\varepsilon_S = 150$ meV, $\varepsilon_W = 300$ meV, and $U = 10$ eV. For this choice of U states S and W cannot be populated simultaneously. The corresponding panels of Figs. 3 and 4 show similar results for the same choice of parameters, except that in Fig. 3 U is taken 500 meV while in Fig. 4 $\Gamma_W^L = 1.9$ meV and $\Gamma_W^R = 0.1$ meV (so $\Gamma_W = \Gamma_W^L + \Gamma_W^R = 2$ meV as before). The latter choice designates level W as a blocking level - current goes down considerably when the voltage bias exceeds the threshold (300 meV) needed to populate it),

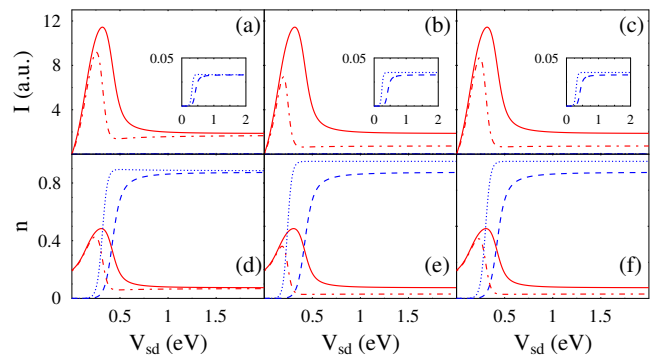


FIG. 4. (Color online) Same as Fig. 2 except $\Gamma_W^L = 1.9$ meV and $\Gamma_W^R = 0.1$ meV.

and has been suggested before⁴⁻⁷ as a model for negative differential resistance in molecular junctions. Finally, in Fig. 5, the parameters are the same as in Fig. 2 except that $T = 0$ K. The voltage was changed by moving the Fermi level of the left electrode, keeping the right electrode static. The insets in the I/V plots show a closeup look at the contribution from channel W . The following observations are notable:

(a) In comparison with the full quantum calculation, Model A performs considerably better than model B and, not surprisingly, than model C. The failure of model B is notable in view of the common practice to use the timescale separation as an argument for applying mean field theory in such calculations; however, as argued above, it follows from the use of the wide band limit for the electrodes in the calculations.

(b) While model A seems to be quite successful in much of the voltage regime, it fails, as expected, near and around $V = 0.3$ V, the (bare) threshold to populate the W level. It is at this point of maximal fluctuations in the W population that electronic correlation is most pronounced, as this population is strongly correlated with that in S .

(c) The deviation of the kinetic approximation from the full quantum result is considerably larger for the current and population of channel W (the redox site) than for channel S . This reflects the fact that the rates of charging and discharging the redox site are sensitive to its correlation with the population on the strongly coupled level, while the dynamics of the latter responds most of the time just to the static population in W . Of course, these large deviations in the current carried by channel W have only an insignificant effect on the overall observed current. To see these important quantum correlation effects one would need to monitor directly the electronic population of the redox site, which is possible in principle using spectroscopy probes.

(d) As a model for negative differential resistance (Fig. 4), model A performs qualitatively well, however the full calculation sets the NDR threshold considerably higher than that predicated by the approximate calculation.

(e) As expected, the differences between the full quan-

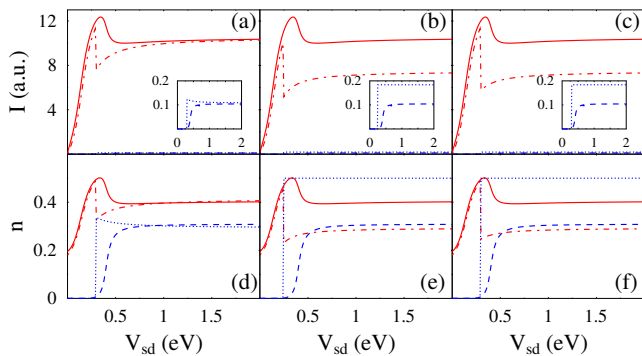


FIG. 5. (Color online) Same as Fig. 2 except $T = 0$ K.

tum calculation and the results of model A become more pronounced at $T = 0$ K. While the results of model A display sharp threshold behavior, the full calculation is much less sensitive to temperature for the present choice of parameters because the width of the transition region is dominated by Γ_S that is substantially greater than the thermal energy.

V. CONCLUSION

We have examined the electronic transport behavior of a generic junction model that comprises a bridge characterized by two interacting transport channels whose couplings to the leads are vastly different from each other. This is a model for a molecular redox junction and also for a point contact detector interacting with a weakly coupled nanodot bridge. We have compared approximate kinetic schemes for the dynamics of this junction to a full quantum calculation based on the pseudoparticle NEGF methodology. We found that a kinetic model in which the electron transfer rates in the weakly coupled channel (redox site) respond instantaneously to occupation changes in the strongly coupled channel works relatively well in comparison with a mean field calculation. Still, this model fails quantitatively when the molecular level comes close to the electrochemical potential of the lead, reflecting the significance of electronic correlations in this voltage range.

This paper has focused on the steady state current. Correlations between the two channels are expected to become considerably more pronounced in the noise properties of such junctions and, most probably, would not be amenable to analysis using the kinetic approximation of model A. We defer this interesting issue to future work.

ACKNOWLEDGMENTS

The research of AN is supported by the Israel Science Foundation, the Israel-US Binational Science Foundation and the European Research Council under the Euro-

pean Union's Seventh Framework Program (FP7/2007-2013; ERC grant agreement no 226628). MG gratefully acknowledges support by the Department of Energy (Early Career Award, DE-SC0006422) and the US-Israel Binational Science Foundation (grant no. 2008282). We thank Kristen Kaasbjerg for useful discussions. MG and AN thank the KITPC Beijing for hospitality and support during the time when this work was completed.

Appendix A: Timescale considerations leading to the models A and B

When it is reasonable to speak about rate of a channel, the formal expression for the W channel rate is??

$$\int_{-\infty}^t dt' e^{i \int_{t'}^t ds \varepsilon_r(s)} V(t) C(t-t') V(t') \quad (\text{A1})$$

where ε_r is the position of the redox level, $V(t)$ is the coupling between the channel W and the bath, and $C(t-t')$ is the bath correlation time.

At least two timescales have to be taken into account: one related to the dynamics of the redox level, $\varepsilon_r(t)$, the other representing characteristic timescale of the bath. Note, that in general the bath is characterized by several timescales (e.g. the bandwidth of the metal, temperature, and variation of spectral density). In our case the characteristic timescale for the dynamics of the level in the W channel is given by the rate of population change in the S channel. The latter is proportional to Γ_S^{-1} (Coulomb interaction is instantaneous). Let assume that the characteristic time of the bath is τ_B . The two extremes are $\tau_B \ll \Gamma_S^{-1}$ and $\tau_B \gg \Gamma_S^{-1}$. The former case corresponds to slow motion of the level relative to the bath dynamics, so that expression (A1) yields a set of rates (2 in our case) for different positions of the redox level. This corresponds to the model A of the paper.

The other extreme, $\tau_B \gg \Gamma_S^{-1}$, corresponds to quick motion of the redox level position, which requires averaging of the exponential factor in (A1). This leads to appearance of a single rate, calculated at the average position of the level, which is model B.

- ¹M. Galperin, M. A. Ratner, and A. Nitzan, *Nano Lett.* **5**, 125-130 (2005).
- ²M. Galperin, A. Nitzan, and M. A. Ratner, *J. Phys.: Condens. Matter* **20**, 374107 (2008).
- ³M. Galperin, A. Nitzan, and M. A. Ratner, arXiv:0909.0915 (2009).
- ⁴M. H. Hettler, H. Schoeller, and W. Wenzel, *Europhys. Lett.* **57**, 571 (2002).
- ⁵B. Muralidharan and S. Datta, *Phys. Rev. B* **76**, 035432 (2007).
- ⁶R. Hartle and M. Thoss, *Phys. Rev. B* **83**, 115414 (2011).
- ⁷A. Migliore and A. Nitzan, *ACS Nano* **5**, 6669 (2011).
- ⁸K. F. Albrecht, H. Wang, L. Mühlbacher, M. Thoss, and A. Komnik, *Phys. Rev. B* **86**, 081412 (2012).
- ⁹It should be emphasized that the theory addresses only locally stable states that will not persist beyond some finite lifetime, and do not imply multistability in the thermodynamic sense.
- ¹⁰M. Field, C. G. Smith, M. Pepper, D. A. Ritchie, J. E. F. Frost, G. A. C. Jones, and D. G. Hasko, *Phys. Rev. Lett.* **70**, 1311 (1993).

- ¹¹J. M. Elzerman, R. Hanson, L. H. W. v. Beveren, B. Witkamp, L. M. K. Vandersypen, and L. P. Kouwenhoven, *Nature* **430**, 431 (2004).
- ¹²L. M. K. Vandersypen, J. M. Elzerman, R. N. Schouten, L. H. W. v. Beveren, R. Hanson, and L. P. Kouwenhoven, *App. Phys. Lett.* **85**, 4394 (2004).
- ¹³R. Schleser, E. Ruh, T. Ihn, K. Ensslin, D. C. Driscoll, and A. C. Gossard, *Appl. Phys. Lett.* **85**, 2005 (2004).
- ¹⁴T. Fujisawa, T. Hayashi, R. Tomita, and Y. Hirayama, *Science* **312**, 1634 (2006).
- ¹⁵S. Gustavsson, R. Leturcq, B. Simovic, R. Schleser, T. Ihn, P. Studerus, K. Ensslin, D. C. Driscoll, and A. C. Gossard, *Phys. Rev. Lett.* **96**, 076605 (2006).
- ¹⁶S. A. Gurvitz and Y. S. Prager, *Phys. Rev. B* **53**, 15932 (1996).
- ¹⁷S. A. Gurvitz, *Phys. Rev. B* **56**, 15215 (1997).
- ¹⁸G. Bulnes Cuetara, M. Esposito, and P. Gaspard, *Phys. Rev. B* **84**, 165114 (2011).
- ¹⁹A. Carmi and Y. Oreg, *Phys. Rev. B* **85**, 045325 (2012).
- ²⁰G. Kiesslich, P. Samuelsson, A. Wacker, and E. Scholl, *Phys. Rev. B* **73**, 033312 (2006).
- ²¹G. Kiesslich, E. Scholl, T. Brandes, F. Hohls, and R. J. Haug, *Phys. Rev. Lett.* **99**, 206602 (2007).
- ²²The “fast” channel carries all the current if the “slow” channel is coupled only to one of the leads.
- ²³A. Migliore, P. Schiff, and A. Nitzan, *Phys. Chem. Chem. Phys.* **14**, 13746 (2012).
- ²⁴B. Muralidharan and S. Datta, *Phys. Rev. B* **76**, 035432 (2007).
- ²⁵M. Leijnse, W. Sun, M. B. Nielsen, P. Hedegard, and K. Flensberg, *J. Chem. Phys.* **134**, 104107 (2011).
- ²⁶K. Kaasbjerg and K. Flensberg, *Phys. Rev. B* **84**, 115457 (2011).
- ²⁷A. Migliore and A. Nitzan, to be published (2013).
- ²⁸P. Coleman, *Phys. Rev. B* **29**, 3035-3044 (1984).
- ²⁹N. E. Bickers, *Rev. Mod. Phys.* **59**, 845-939 (1987).
- ³⁰M. Eckstein and P. Werner, *Phys. Rev. B* **82**, 115115 (2010).
- ³¹J. H. Oh, D. Ahn, V. Bubanja, *Phys. Rev. B* **83**, 205302 (2011).
- ³²M. H. Hettler, J. Kroha and S. Hershfield, *Phys. Rev. B* **58**, 5649-5664 (1998).
- ³³T. Schauerte, J. Kroha, and P. Wölfle, *Phys. Rev. B* **62**, 4394-4402 (2000).
- ³⁴N. S. Wingreen and Y. Meir, *Phys. Rev. B* **49**, 11040-11052 (1994).
- ³⁵N. Sivan and N. S. Wingreen, *Phys. Rev. B* **54**, 11622-1629 (1996).
- ³⁶A. J. White and M. Galperin, *Phys. Chem. Chem. Phys.* **14**, 13809-13819 (2012).
- ³⁷A. J. White, B. D. Fainberg, and M. Galperin, *J. Phys. Chem. Lett.* **3**, 2738-2743 (2012).
- ³⁸Note that while in quantum mechanics damping rates and level widths are synonymous, it is exactly the energetic consequence of the finite lifetime, that is, the level broadening, which is disregarded in the kinetic approximation.
- ³⁹S. Datta, *Electric transport in Mesoscopic Systems* (Cambridge University Press, Cambridge, 1995).
- ⁴⁰H. Haug and A.-P. Jauho, *Quantum Kinetics in Transport and Optics of Semiconductors* (Springer, 2008).
- ⁴¹M. Esposito and M. Galperin, *Phys. Rev. B* **79**, 205303 (2009).